Published in final edited form as:
Kumru, B., Cruz, D., Heil, T., & Antonietti, M. (2020). In situ formation of arrays of tungsten single atoms within carbon nitride frameworks fabricated by one-step synthesis through monomer complexation. Chemistry of Materials, 32(21), 9435-9443. doi:10.1021/acs.chemmater.0c03616.

In situ formation of arrays of tungsten single atoms within carbon nitride frameworks fabricated by one-step synthesis through monomer complexation

B. Kumru, D. Cruz, T. Heil, M. Antonietti

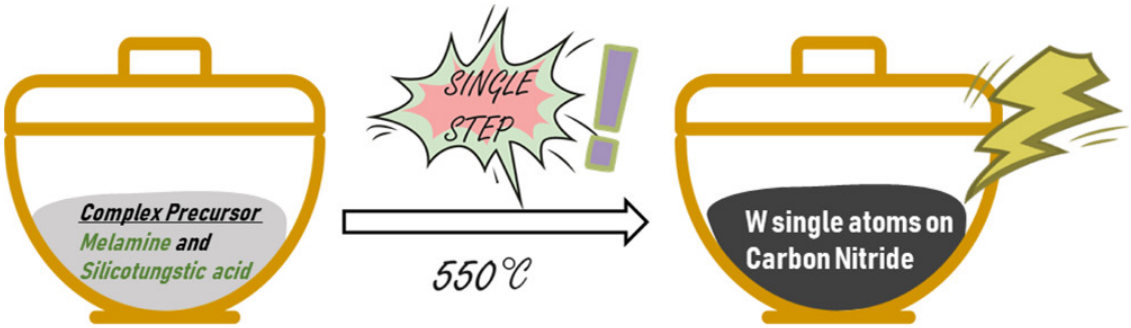

Article

In Situ Formation of Arrays of Tungsten Single Atoms within Carbon Nitride Frameworks Fabricated by One-Step Synthesis through Monomer Complexation

Baris Kumru,* Daniel Cruz, Tobias Heil, and Markus Antonietti*

ABSTRACT: Deposition of stable single atoms on supports is a hot topic, especially for catalysis, and single atom deposition in nitrogen-framed pores of carbon and carbon nitrides is indeed the most successful. The polymeric semiconductor graphitic carbon nitride (g-CN) is an exciting scaffold due to its nitrogen-rich structure (C_3N_4 ideally) and the inherent nitrogen-lined pores, which made the whole, structurally diverse g-CN family an attractive choice for heterogeneous catalysis and photocatalysis. Herein, we present the simple thermal treatment of a monomer complex between melamine and silicotungstic acid to yield massive amounts of tungsten single atoms within the carbon nitride framework. The morphology and photophysical properties of the novel semiconductor with a band gap around 2 eV are investigated in dependence of the tungsten content, and the onset of W−W exchange interactions will be described. Due to the ease of W to change the oxidation state and to bind to oxygen atoms, the material turns out to be an effective catalyst for oxidation reactions, which was exemplified with new oxidative photopolymerization of guaiacol to form artificial lignin-like polyphenols.

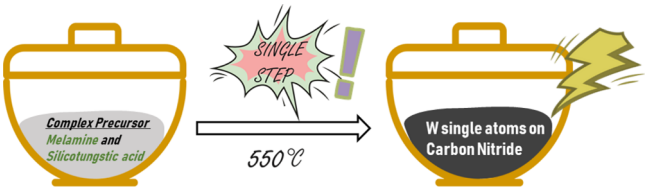

Semiconductors promise a bright future to transform chemical reactions into light-driven analogues, yet most metal-based semiconductors fail from a sustainability perspective despite efficiencies.[1] Polymeric graphitic carbon nitride (g-CN) has been a rising star in recent years due to its metal-free nature and ease of tunability, in addition to its low-cost and nontoxicity.[2] Nitrogen-rich and abundant precursors, that is, melamine, urea, and thiourea, can be condensed at temperatures above 500 °C to yield polymerized and conjugated structures that are photoactive, which have been employed as heterogeneous photocatalysts for water splitting,[3−5] CO_2 reduction,[6−8] organic synthesis,[9−11] pollutant degradation,[12,13] and polymer initiation.[14−17] Nevertheless, there is a big room for improvement of these materials; therefore, modifications are generally applied.[18] In order to tailor the band gap and morphology of g-CN to enhance photocatalytic efficiency, many methods are suggested, which can be subdivided into pre- or postmodification.[19] For instance, the supramolecular assembly method aims to pretreat the precursors in a suitable solvent to form ordered aggregates, which subsequently induce morphology alteration and enhanced photoefficiencies in the resulting g-CN materials.[20−22] The salt-melt method was introduced to yield ordered g-CN materials by providing solvent (salt melt) conditions at synthesis temperatures.[23,24] Acid treatment of basic monomers has been used as a modular tool to tailor the morphology and activity of g-CN.[25,26] Hence, a great potential to integrate novel structures into two-dimensional sheets by premodification lies within this still rather undeveloped strategies.[27]

Inherent photocatalytic activity of g-CN suffers from recombination losses, which can be partially improved via metal deposition on the g-CN surface.[28] As a postmodification method, atom deposition generally encompasses metal precursors (H_2PtCl_6 and[29,30] $HAuCl_4$[31,32]) being treated in g-CN dispersion to form metal clusters or single atoms on the g-CN surface.[33] Alternatively, a very recent article demonstrated a single-step cobalt single atom incorporation into a carbon nitride framework by in situ formation of cobalt chelating active sites on carbon nitride pores, which results in improved photocatalytic efficiencies.[34] A similar complex condensation was reported to attain iron single atoms dispersed in carbon nitride pores, which relies on in situ chelation at condensation temperatures.[35] Silver single atoms can be introduced to a carbon nitride framework in a similar manner as well.[36] Electronic interactions between nitrogen and metal atoms hold the system together, as illustratively depicted for a nitrogen-doped carbon skeleton.[37] Significantly improved photoactivities can be observed as excited electrons migrate to the metal surface which lowers the recombination rate.[38]

Tungsten has been reported to have a profound effect when combined with g-CN, and usually, more efficient photo-

catalysis is obtained. Typically, WO_3 can be physically mixed with g-CN to form composite photocatalysts;[39−41] alternatively, thermal treatment of a tungsten precursor with as-prepared g-CN can yield WO_3−g-CN photoactive composites that are dominated by physical interactions.[42,43] Small atoms such as boron,[44] phosphorus,[45] and sulfur[46] could be covalently introduced into a g-CN network, yet stable introduction of relatively large transition metals into the g-CN repeating motif is unknown.

Herein, an innovative, well-defined complex precursor based on the acid−base assembly of melamine and silicotungstic acid (SiWA, $H_4SiW_{12}O_{40}$) is utilized to synthesize the composite g-CN material in a single thermal condensation step, and the resulting catalysts will be investigated for morphological and photophysical properties.

RESULTS AND DISCUSSION

SiWA is a member of the polyoxometalate (POM, heteropolyacid) family, which shows Keggin-type coordination in aqueous conditions.[47] SiWA is known as a solid-state catalyst (then supported on inert surfaces) for transformation of molecules,[48−51] and it was chosen in the present context as a precursor due to its tungsten-rich structure (12 W-atoms per cluster). Melamine−SiWA (10:4 g, 0.08:0.001 mol) was mixed in water overnight and dried afterward. Acid−base interactions allow small melamine molecules to surround large acidic Keggin ions, therefore providing a joint contact between both components. The thermal condensation of the homogeneous, crystalline complex at 550 °C yielded tungsten containing CN materials (denoted as CN−WA, details in the Methods section, Scheme S1). A reference sample was synthesized utilizing melamine as the sole precursor with the same treatment (denoted as ref-CN). The first visible evident for an altered structure was the appearance of the catalyst powders (Figure 1); the typical yellow color of g-CN was turned into dark brown after tungsten incorporation.

In addition to the obvious color change, typical photoluminescence of g-CN was quenched after tungsten incorporation which can be demonstrated via digital images of the powders shown in Figure 1 under UV light (Figure S1). In order to estimate the thermal development of the condensation reaction, thermogravimetric analysis (TGA) was performed for the melamine−SiWA precursor mixture. TGA exhibits two steep mass loss steps due to polycondensation and stabilizes after 500 °C, and the synthesis at 550 °C seems reasonable, with 23% mass remaining in the condensation product (Figure S2, yield can differ and depends on the setup as TGA and thermal condensation occur under different conditions). As a visual reference, condensation of pure SiWA and the melamine−SiWA physical mixture (without joint crystallization) was conducted at the same temperature, and the resulting materials are green, crystalline, and non-homogenous powders, as shown in Figure S3, which underline the necessity of molecular mixing by binary preorganization. It is also important to mention that lower SiWA loading is not sufficient for the formation of a brown nanocomposite (data not shown) and that a 10:4 melamine−SiWA (g/g) ratio was found to be optimum to generate this new electronic state.

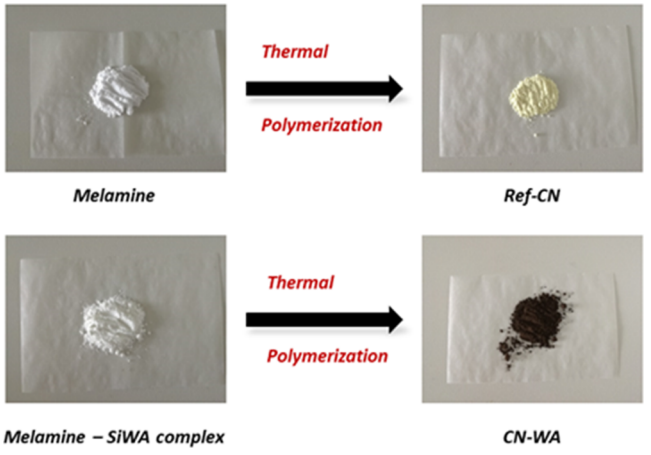

Figure 1. Digital images of melamine and the resulting ref-CN sample (top), melamine−SiWA complex, and resulting CN−WA sample (bottom).

UV−vis spectra of ref-CN revealed the standard g-CN absorption profile (Figure 2a), with a band gap of 2.73 eV, as calculated from the Tauc plot (Figure 2a inlet). Significant enhancement in absorption (corresponding to higher transition moment) as well as a shift of the band gap toward the red was obtained for the CN−WA sample, where the Tauc plot (Figure 2a) gave a band gap value of 2.05 eV or about 600 nm (Figure 2a inlet), which is evident that tungsten incorporation alters the light absorption capacity of the resulting hybrid. Photoluminescent (PL) spectra of both samples were acquired from aqueous dispersions (Figure 2b), and photoluminescence is largely quenched after tungsten incorporation, supporting the previously discussed visual observation (Figure S1). The minor leftover fluorescence seems to be similar to original g-CN, and no W-hybrid-related transitions are seen in fluorescence (than expected at longer wavelengths).

The X-ray diffraction (XRD) profile of ref-CN (Figure 2c-inlet) exhibits a peak around 13° and a sharp peak around 27°, which are comparable to the literature values of traditional g-CN materials. The XRD profile of CN−WA (Figure 2c) shows a broad peak. As in this hybrid, most of the X-ray scattering is essentially due to tungsten, reflecting that the tungsten atoms are not mutually ordered, but rather amorphous within the hybrid structure, which will be discussed later. XRD of the SiWA monomer (Figure S4) and melamine−SiWA complex (Figure S5) indicates highly crystalline structures for both cases, and changes in the diffractograms are found after complex formation (peak formation at 18°, enhanced peaks at a range of 25−30°, and pronounced decrease of peak intensities after 40°), representing that melamine and SiWA indeed recrystallize as a joint complex. Calcination of pure SiWA at 550 °C gives a similar profile to annealed WO_3[52], with slight differences due to the contained silica (Figure S6), and it is important to mention that it has a strong green color that differs from WO_3 which is yellow, a change typical for oxygen vacancies. XRD curves of the carbonized melamine−SiWA physical mixture (Figure S7) resemble g-CN diffractograms, yet the sample was nonhomogeneous (Figure S3-right), while the XRD sample was taken from the top of the crucible (presumably g-CN rich). Fourier transform infrared (FT-IR) spectra of precursors were investigated in order to obtain a hint after joint crystallization. After complexation, amino vibrations from melamine are attained (though weakened compared to pure melamine) as well as the fingerprint region from SiWA is detectable in the complex precursor. In addition, a region that is related to aromatic vibrations arising from melamine was observed (Figure S8). The scanning electron microscopy

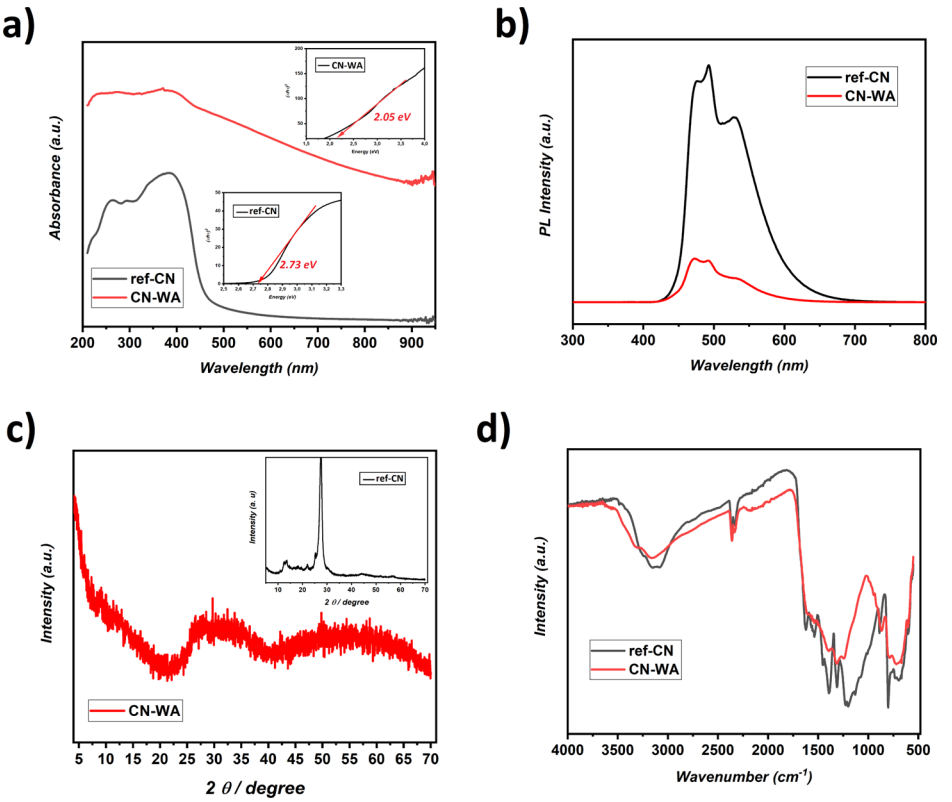

Figure 2. (a) UV−vis spectra of ref-CN and CN−WA samples (inlets demonstrating Tauc plots), (b) PL spectra of ref-CN and CN−WA samples, (c) powder XRD profiles of CN−WA and ref-CN (inlet), (d) FT-IR spectra of ref-CN and CN−WA samples.

(SEM) image of the mel−SiWA complex visualizes a crystalline complex structure (Figure S9). FT-IR spectra of ref-CN highlights the vibrations arising from the CN heterocycle, C−N, and C═N, as well as $-NH_2$ at 810, 1250−1350, 1560, and 3200 cm^{-1} respectively (Figure 2d). Similar spectra are obtained for CN−WA; however, the sharpness of the aforementioned peaks is missing, which indicates coupling of heavy W to the framework in an irregular fashion.

Ref-CN has a hollow tubular-like structure as identified by SEM (Figure S10). This is typical for preorganized complexes as starting products, as, for instance, melamine itself is reported to undergo self-assembly throughout pretreatment in water leading to hollow pipe-like morphologies.[53] CN−WA possesses quite a uniform structure with high homogeneity (Figure 3a), unlike the macroscopic WO_3−g-CN composites mentioned in the literature.[39,40] The physical composites made before have two distinct regions that are easily identifiable as a g-CN network and WO_3 deposited on top. In our case, a material with a single morphology was obtained. Elemental mapping via SEM exhibits uniform distribution of C, N, O, and W atoms over the whole sample (Figure S11), and energy dispersive X-ray (EDX) spectra confirm the C, N, O, and W atoms in the CN−WA sample (Figure S12).

Composition of both samples was investigated as shown in Table 1. Combustive elemental analysis of ref-CN revealed the nitrogen-rich network with the $C_3N_{4.4}$ molar ratio, and a similar method was attempted for CN−WA, but the sample does not have a tendency to combust. Therefore, EDX analysis was utilized for the estimation of the elemental composition of the CN−WA sample, which gave a $C_3N_{4.35}W_{0.38}O_{1.06}$-type structure from an average of five independent areas. The

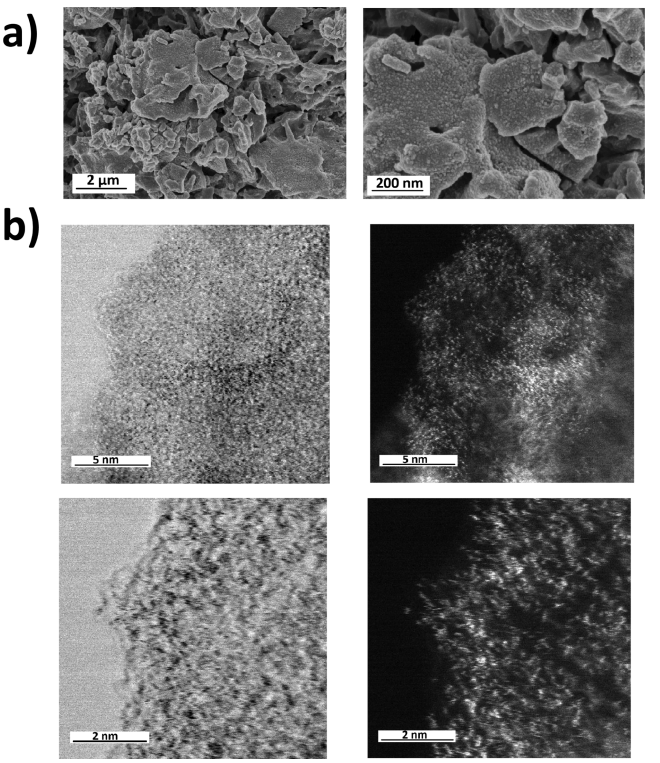

Figure 3. (a) SEM images of the CN−WA sample, (b) scanning transmission electron microscopy (STEM) brightfield (left) and darkfield (right) images at atomic resolution of the CN−WA sample.

weight percent of tungsten is quite high in CN−WA, but it is important to keep in mind that the atomic mass of tungsten is

Table 1. Elemental Composition and Surface Areas of Ref-CN and CN−WA Samples

Sample	C (wt %)	N (wt %)	O (wt %)	W (wt.%)	C/N ratio	formula	surface area[d] (m^2 g^{-1})
Ref-CN	35.7[a]	61[a]			0.65[a]	$C_3N_{4.4}$[c]	22
CN−WA	19.8[b]	33.4[b]	9.3[b]	37.4[b]	0.69[b]	$C_3N_{4.35}W_{0.38}O_{1.06}$[c]	4

[a]Obtained via combustive elemental analysis. [b]Obtained via the average of five independent measurements by SEM EDX analysis. [c]Calculated via the conversion of weight of elements to molar portions. [d]Obtained via the nitrogen desorption method using BET to evaluate data.

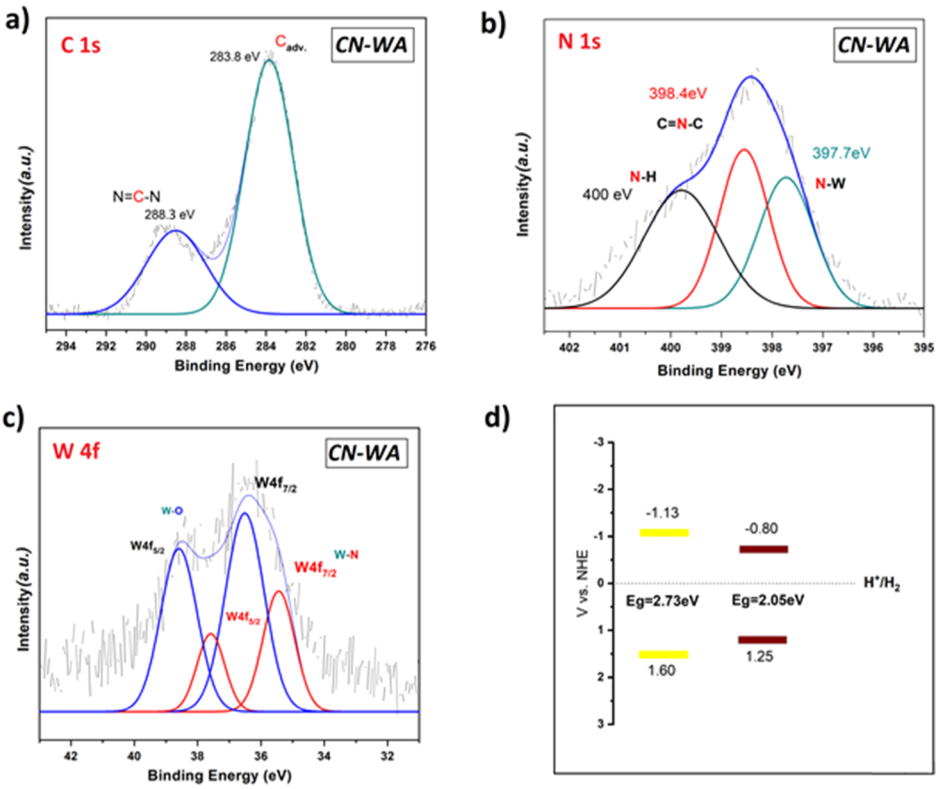

Figure 4. XPS survey of the CN−WA sample: (a) C 1s, (b) N 1s, and (c) W 4f core levels, (d) band gap diagrams of ref-CN and CN−WA samples (with respect to the standard hydrogen electrode).

higher than those of the other elements. In addition, the ICP method presented 33 wt % tungsten atom in the sample; such a high atomic ratio can be attributed to high temperatures and single-step in situ synthesis conditions from the joint crystallized precursor, which differs from the post-atom deposition methods. It is also important to bear in mind that EDX is an area-oriented method; therefore, the elemental ratios are approximities. Surface area measurement by the nitrogen desorption method using the BET method demonstrated 22 m^2 g^{-1} for ref-CN and 4 m^2 g^{-1} for CN−WA. All these point to a rather unperturbed CN-condensation, with about one W atom per two heptazine pores, potentially stacked on top of each other.

High-resolution transmission electron microscopy (HR-TEM) and STEM measurements were utilized to gain insights into the atomistic structures of both samples. HR-TEM of ref-CN exposes sheet-like structures that are similar to traditional g-CNs (Figure S13). HR-TEM of CN−WA divulges a surprising structure (Figure 3b); the whole system is homogeneous (as also observed in SEM), while tungsten single atoms are observed in dark field images at atomic resolution. This is unusual for a content of 37 wt % but was reasoned before to be the result of the pore structure of g-CN. On top, the isolated W-atoms seem to have no mutual organization but are rather randomly distributed in the sample, thus confirming the XRD data. TEM results of g-classical, macroscopic CN, and WO_3 composites from the literature[41] clearly indicate two different morphologies rather than a single material, which confirms the formation of a physical composite mixture.

In our case, a homogeneous network and distribution of tungsten single atoms/clusters hint toward the formation of a novel "alloy type" material[54] based on tungsten and the carbon nitride framework. In order to confirm structures, more HR-TEM measurements were performed on the CN−WA sample together with corresponding electron energy loss spectroscopy (EELS) spectra. All four additional measurements (Figures S14,S16,S18,S20) exhibit a similar morphology; a uniform network is visible at lower magnification, and dark field images at an atomic scale reveal tungsten single atoms/clusters. Each corresponding EELS spectra (Figures S15,S17,S19,S21) confirm the presence of W in the investigated area, supporting the claim that the visible atoms of heavier elements are indeed tungsten. However, doubling the amount of SiWA in the complex precursor resulted in a completely altered morphology of the final material (Figures S22,S23). HRTEM revealed a significant phase demixing for the CN−2WA sample, where the heavier element (tungsten) lines up and forms a distortion within a g-CN framework, resulting in a sand wave-like

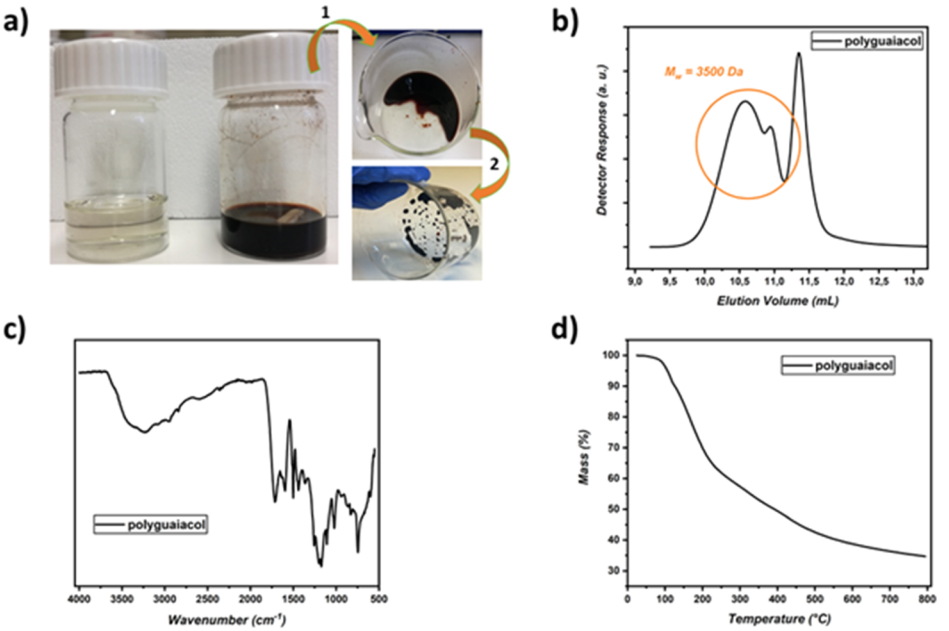

Figure 5. (a) Digital images of samples; the left vial is a solution before reaction (without CN−WA addition), and the right vial is after photooxidative polymerization. Pathway 1 is after filtration, and pathway 2 is after drying. (b) SEC elugram of polyguaiacol obtained in basic water calibrated with PSSNa standards, (c) FT-IR spectra of polyguaiacol, (d) TGA result of polyguaiacol.

assembly. Therefore, we have not investigated this sample further.

XPS was performed in order to understand the nature of surface chemistry and bonding in samples. Ref-CN consists of a typical CN heterocycle (C 1s and N 1s core levels, Figure S24) with binding energies that are consistent with the literature.[55] Similar patterns were obtained for the CN−WA sample with the C and N 1s core levels, with a surprise of peak shifts (Figure 4a,b). Such a phenomenon was previously reported when our group attempted vinyl thiazole grafting to g-CN, in which the electrons migrated to vinyl thiazole groups, and similar changes in XPS survey were reported.[56,57] In this case, both peaks from the carbon core are shifted to negative values (around −0.4 eV), and a peak from the nitrogen core (of g-CN) is shifted by +0.3 eV, which indicates a change in the electron density over carbon nitride frameworks after tungsten incorporation. A change in electronic density after metal incorporation into a host network has been attributed to charge transfer-induced stabilization,[37,58] as dentate-like nitrogen pots can transfer electrons to stabilize the guest metal particles. Indeed, the nitrogen moieties turn more electron poor due to electron donation to W, while the carbon atoms are more electron-rich, to compensate the partial charge on the neighboring nitrogen atoms. This essentially complies with the rule of alternating electron polarizations in joint wave functions. Such stabilization, in general, renders improved catalytic activity as well, as the so-formed Schottky dyad improves Fermi level equilibration and charge separation.[58]

The electronic-state difference of nitrogen atoms in ref-CN and CN−WA was further followed via EELS spectra by HR-TEM (Figure S25), which shows earlier onset and a more positive nature of nitrogen atoms in CN−WA and the ones in ref-CN. Furthermore, N 1s of CN−WA reveals the N−W bond (Figure 4b), and W 4f spectra show W−O and W−N bonds that are positioned quite different from WO_3[59] and WN[60] on nitrogen-rich carbon-based frameworks. Tungsten is known to form complex architectures in the presence of nitrogen donors,[61] yet the capacity of g-CN as a multiple chelating donor has not been explored previously. Clearly, all data support our view that the SiWA clusters are broken up and inject tungsten single ions into the carbon nitride framework.

UPS survey (Figure S26) was conducted in order to comprehend the band gap of samples (Figure 4d). A significant increase in intensity, that is, density of states, was obtained for CN−WA compared to ref-CN, and lower work function value (3.2 eV for CN−WA and 3.9 eV for ref-CN) after tungsten incorporation indicates lower energetic barriers and hence easier flow of electrons.[62] All these results combined hint toward the formation of a uniform material (tungsten in the carbon nitride framework) thus eliminating other possibilities which assume the formation of two distinct layers (i.e. WN formation on carbon) since WN itself has quite different characteristics (i.e. crystallinity, work function, and band gap).[63]

These band positions of the material and the known oxygen activating character of tungsten make it suitable as a potentially very selective oxidation catalyst, similar to a peroxidase enzyme. Our current interest in such selective oxidation reactions is mostly along biobased degradable polymers, for example, the build-up and the degradation of lignin (here then called ligninase, as known from fungi). There is a general interest for polymerization of small aromatic molecules to understand how lignin is constructed in nature, which is generally attributed to oxidative polymerization of aromatic molecules such as guaiacol or monolignols.[64] Complex C−O and C−C coupling governed by natural enzymes which activate hydrogen peroxide can be the key steps in such oxidative polymerization.

Guaiacol was polymerized before via enzymes and is considered to be the simplest lignin model.[65] We have chosen guaiacol as a simple model compound and performed the photocatalytic oxidation reaction as delineated in the Methods section. It is important to note that the reaction in the absence

of hydrogen peroxide does not proceed, which already hints toward enzyme-like activation of H_2O_2 by the CN−WA catalyst as the key driver of the polymerization reaction.

The color of the reaction media turns blackish after 6 h reaction (Figure 5) and really looks and behaves as "lignin black liquor". The solution was then filtered to remove the photocatalyst (Figure 5, pathway 1) and dried (Figure 5, pathway 2). In other previous reports, guaiacol is reported to undergo cyclization (O−O coupling) to form tetramer units (molecular weight 456 g mol^{-1}) via peroxidase,[66] the known guaiacol oxidation assay. We have conducted size exclusion chromatography (SEC), which shows broad molecular mass distribution of a polymer with an average of 3500 Da, which is rather typical for lignins. FT-IR spectra of polymers show a broad peak around 3450 cm^{-1} attributed to the phenolic hydroxyl groups (Figure 5c). More pronounced peak clusters between 1400 and 1600 cm^{-1} are attributed to aromatic rings, and a slight peak at 1750 cm^{-1} can be due to partial phenol oxidation during oxidative polymerization. The peak at 1030 cm^{-1} represents C−H in plain deformation, and peaks around 1200 cm^{-1} present vibration of guaiacyl rings.[67] The TGA diagram of the polymer sample is similar to the one of kraft lignin,[67] a curve with a gradual decrease over a broad temperature range, which results 37% mass at 800 °C indicating the formation of carbonaceous species (Figure 5d). As control experiments, ref-CN or the mel−SiWA complex did not produce any polymer (not even a color change in reaction media), indicating that the oxidative power of these materials is not sufficient enough to conduct guaiacol polymerization via H_2O_2 photoactivation.

The solubility and processability of polyguaiacol, unlike natural crosslinked polymers, and the simplified non-enzymatic synthesis together with the known redox properties of polyphenols as well as their ability to bind ions point to a rich potential application spectrum, which however is out of the scope of the present paper.

CONCLUSIONS

A crystalline, acid−base-induced complex of silicotungstic acid and melamine was introduced as a promising precursor for thermal condensation toward a novel semiconductor containing tungsten single atoms. The obtained structure was characterized via HR-TEM, SEM, XPS, and UPS which elucidated morphological and photophysical properties. Entailing such a large transition metal into the g-CN network is highly interesting from a coordination chemistry view of tungsten, and the novel fused composite material is photoactive and easily scalable and reproducible.

Tungsten single atoms were imaged by STEM imaging at an atomic scale, and a corresponding change in the electronic state as well as photophysical properties was discussed via XPS and UPS. A narrowed band gap after tungsten incorporation promises a wider use of solar light and that the oxidation potential is smoothened, promising to move from deep oxidation to selective oxidation. This together with the known properties of W to act as a local binding site for substrates assures broader application. The peroxidase-like activity of the materials was illustrated by a sensitive model reaction and the photo-oxidative polymerization of guaiacol, and a soluble polymer with a molecular weight of 3500 g mol^{-1} was obtained which can be understood as a simplified lignin model.

From a materials design perspective, we believe that such a simple methodology could be extended to other metal systems, and the facile recipe could significantly influence catalysis by simple and effective fabrication of single atoms containing scaffolds in broader range than done before.

METHODS

Materials. All chemicals were used as purchased. Ethanol (absolute, Merck), guaiacol (98%, Sigma-Aldrich), hydrogen peroxide (30 wt % solution, Sigma-Aldrich), melamine (99%, Alfa Aesar), and silicotungstic acid (Sigma-Aldrich) were used.

Synthesis of CN−WA. 10 g of melamine and 4 g of silicotungstic acid (SiWA) powders were mixed in 50 mL of distilled water overnight and dried in an oven at 80 °C until complete water evaporation. The resulting powder (melamine−SiWA complex) is placed in a capped aluminum crucible and heated up to 550 °C (4 h to reach 550 °C and another 4 h at 550 °C) under a nitrogen-protected oven. After cooling down, the catalyst is washed with water overnight, filtered, and dried (the catalyst is denoted as CN−WA). It is important to note that the doping effect is activated in a 10:4 mixing ratio and not in lower ratios.

Synthesis of CN−2WA. 10 g of melamine and 8 g of silicotungstic acid (SiWA) powders were mixed in 50 mL of distilled water overnight and dried in an oven at 80 °C until complete water evaporation. The resulting powder (melamine−SiWA complex) is placed in a capped aluminum crucible and heated up to 550 °C (4 h to reach 550 °C and another 4 h at 550 °C) under a nitrogen-protected oven. After cooling down, the catalyst is washed with water overnight, filtered, dried (the catalyst is denoted as CN−2WA), and subjected to HR-TEM investigation.

Synthesis of Ref-CN. 10 g of melamine is utilized as a precursor and mixed with 50 mL of distilled water overnight and dried in an oven at 80 °C until complete water evaporation. The resulting powder is placed in a capped aluminum crucible and heated up to 550 °C (4 h to reach 550 °C and kept 4 h at 550 °C) under a nitrogen-protected oven. After cooling down, the catalyst is washed with water overnight, filtered, and dried (the catalyst is denoted as ref-CN).

Oxidative Polymerization of Guaiacol. 50 mg of CN−WA was employed with 1 mL of guaiacol, 3 mL of ethanol, and 0.2 mL of hydrogen peroxide solution. Reaction was irradiated via visible light for 6 h and filtered, and the solute was dried in a vacuum oven at 60 °C overnight. As reference experiments, CN−WA was replaced with either ref-CN or the mel−SiWA complex; however, no polymer formation was observed for both cases.

Characterization. Powder XRD patterns were obtained using a Bruker D8 ADVANCE X-ray diffractometer via Cu Kα radiation. SEM and EDX elemental mapping were performed using JEOL JSM-7500F equipped with an Oxford Instruments X-MAX 80 mm^2 detector for the determination of the morphology. Solid-state ultraviolet−visible (UV−vis) spectroscopy for powder catalysts was recorded via a Cary 500 scan spectrophotometer equipped with an integrating sphere. FT-IR spectra were taken on a Nicolet iS 5 FT-IR spectrometer. Combustive elemental analysis of CN−WA and ref-CN was performed via a Vario Micro device. PL emission spectra were recorded on a Jasco FP-8300 instrument at ambient temperature using aqueous dispersions of catalysts with the excitation wavelength at 360 nm. HR-TEM, STEM, EDX, and EELS measurements were acquired using a double-Cs-corrected Jeol ARM200F, equipped with a cold field emission gun and a Gatan GIF Quantum and operated with an acceleration voltage of 200 kV. The tungsten atom content was further analyzed by inductively coupled plasma optical emission spectroscopy (ICP-OES) using an Optima 8000 ICP-OES from PerkinElmer. 0.2 mg of CN−WA sample was well grinded and digested in aqua regia for 5 h prior to measurement. SEC was conducted in water by dissolving the polymer in basic water at 25 °C using a column system composed of a PSS SDV 1000/10,000/1,000,000 column (8 × 300 mm, 5 μm particle size) with a PSS SDV precolumn (8 × 50 mm), a SECcurity RI detector, and a SECcurity UV−vis detector and calibration with PSSNa standards from PSS.

The core levels of C 1s, N 1s, and W 4f in catalyst samples were studied with XPS measurements using CISSY equipment in ultrahigh vacuum, with SPECS XR 50 X-ray gun Mg Kα radiation (1254.6 eV) and a combined lens analyzer module. Valence band maximum was analyzed with UPS and carried out with a excitation source of He I 21.2 eV radiation and UVS 10/35, and the data were acquired at a bias −10 V. The calibration was performed by the Fermi level of the gold reference sample. TGA was performed via TG 209 Libra from NETZSCH in a nitrogen atmosphere with a heating rate of 10 K min^{-1} using an aluminum crucible for samples.

■ ASSOCIATED CONTENT

Supporting Information

The Supporting Information is available free of charge at https://pubs.acs.org/doi/10.1021/acs.chemmater.0c03616.

Illustration of melamine-silicotungstic acid complexation and the final CN-WA material; digital images of melamine, ref-CN, mel-SiWA complex, and CN-WA powders; TGA results; digital images of thermally treated SiWA and SiWA-melamine; XRD patterns; FT-IR spectra of samples; SEM images and elemental mapping of the mel-SiWA complex, ref-CN, and CN−WA; additional HRTEM measurements; EDX spectra; STEM images; background-subtracted EELS spectra; and XPS spectra of ref-CN and UPS survey of the samples (PDF)

■ AUTHOR INFORMATION

Corresponding Authors

Baris Kumru − *Max Planck Institute of Colloids and Interfaces, Potsdam 14424, Germany;* orcid.org/0000-0002-1203-4019; Email: baris.kumru@mpikg.mpg.de

Markus Antonietti − *Max Planck Institute of Colloids and Interfaces, Potsdam 14424, Germany;* orcid.org/0000-0002-8395-7558; Email: office.cc@mpikg.mpg.de

Authors

Daniel Cruz − *Max Planck Institute of Colloids and Interfaces, Potsdam 14424, Germany*

Tobias Heil − *Max Planck Institute of Colloids and Interfaces, Potsdam 14424, Germany*

Complete contact information is available at: https://pubs.acs.org/10.1021/acs.chemmater.0c03616

Author Contributions

B.K. and M.A. conceived the idea and designed the experiments. B.K. conducted experiments. D.C performed photophysical characterizations, and T.H. performed the detailed TEM characterizations. The manuscript was written through contributions of all authors. All authors have given approval to the final version of the manuscript.

Notes

The authors declare no competing financial interest.

■ ACKNOWLEDGMENTS

The authors greatly acknowledge the Max Planck Society for funding. Heike Runge is greatly acknowledged for SEM measurements, Antje Voelkel for TGA and elemental analysis measurements, and Marlies Graewert for SEC measurement. Dr. Majd Al-Naji and Dr. Paolo Giusto are acknowledged for fruitful coffee discussions. We thank PvComB-Helmholtz Zentrum Berlin and Dr. Iver Lauermann for XPS and UPS access.

■ REFERENCES

(1) Hu, C.; Lin, Y. R.; Yang, H. C. Recent Developments in Graphitic Carbon Nitride Based Hydrogels as Photocatalysts. *ChemSusChem* **2019**, *12*, 1794−1806.

(2) Liu, J.; Wang, H.; Antonietti, M. Graphitic carbon nitride "reloaded": emerging applications beyond (photo)catalysis. *Chem. Soc. Rev.* **2016**, *45*, 2308−2326.

(3) Peng, G.; Albero, J.; Garcia, H.; Shalom, M. A Water-Splitting Carbon Nitride Photoelectrochemical Cell with Efficient Charge Separation and Remarkably Low Onset Potential. *Angew. Chem., Int. Ed.* **2018**, *57*, 15807−15811.

(4) Xiong, W.; Huang, F.; zhang, R.-Q. Recent developments in carbon nitride based films for photoelectrochemical water splitting. *Sustainable Energy Fuels* **2020**, *4*, 485−503.

(5) Han, Q.; Wang, B.; Zhao, Y.; Hu, C.; Qu, L. A Graphitic-C3N4 "Seaweed" Architecture for Enhanced Hydrogen Evolution. *Angew. Chem., Int. Ed.* **2015**, *54*, 11433−11437.

(6) Kuriki, R.; Sekizawa, K.; Ishitani, O.; Maeda, K. Visible-Light-Driven CO2 Reduction with Carbon Nitride: Enhancing the Activity of Ruthenium Catalysts. *Angew. Chem., Int. Ed.* **2015**, *54*, 2406−2409.

(7) Huang, P.; Huang, J.; Pantovich, S. A.; Carl, A. D.; Fenton, T. G.; Caputo, C. A.; Grimm, R. L.; Frenkel, A. I.; Li, G. Selective CO_2 Reduction Catalyzed by Single Cobalt Sites on Carbon Nitride under Visible-Light Irradiation. *J. Am. Chem. Soc.* **2018**, *140*, 16042−16047.

(8) Zhao, G.; Pang, H.; Liu, G.; Li, P.; Liu, H.; Zhang, H.; Shi, L.; Ye, J. Co-porphyrin/carbon nitride hybrids for improved photocatalytic CO2 reduction under visible light. *Appl. Catal., B* **2017**, *200*, 141−149.

(9) Kumru, B.; Mendoza Mesa, J.; Antonietti, M.; Al-Naji, M. Metal-Free Visible-Light-Induced Dithiol−Ene Clicking via Carbon Nitride to Valorize 4-Pentenoic Acid as a Functional Monomer. *ACS Sustainable Chem. Eng.* **2019**, *7*, 17574−17579.

(10) Ghosh, I.; Khamrai, J.; Savateev, A.; Shlapakov, N.; Antonietti, M.; König, B. Organic semiconductor photocatalyst can bifunctionalize arenes and heteroarenes. *Science* **2019**, *365*, 360−366.

(11) Cavedon, C.; Madani, A.; Seeberger, P. H.; Pieber, B. Semiheterogeneous Dual Nickel/Photocatalytic (Thio)etherification Using Carbon Nitrides. *Org. Lett.* **2019**, *21*, 5331−5334.

(12) Zheng, Q.; Durkin, D. P.; Elenewski, J. E.; Sun, Y.; Banek, N. A.; Hua, L.; Chen, H.; Wagner, M. J.; Zhang, W.; Shuai, D. Visible-Light-Responsive Graphitic Carbon Nitride: Rational Design and Photocatalytic Applications for Water Treatment. *Environ. Sci. Technol.* **2016**, *50*, 12938−12948.

(13) Ai, B.; Duan, X.; Sun, H.; Qiub, X.; Wang, S. Metal-free graphene-carbon nitride hybrids for photodegradation of organic pollutants in water. *Catal. Today* **2015**, *258*, 668−675.

(14) Kaya, K.; Kiskan, B.; Kumru, B.; Schmidt, B. V. K. J.; Yagci, Y. An oxygen-tolerant visible light induced free radical polymerization using mesoporous graphitic carbon nitride. *Eur. Polym. J.* **2020**, *122*, 109410.

(15) Kumru, B.; Molinari, V.; Hilgart, M.; Rummel, F.; Schäffler, M.; Schmidt, B. V. K. J. Polymer Grafted Graphitic Carbon Nitride as Precursors for Reinforced Lubricant Hydrogels. *Polym. Chem.* **2019**, *10*, 3647−3656.

(16) Yandrapalli, N.; Robinson, T.; Antonietti, M.; Kumru, B. Graphitic Carbon Nitride Stabilizers Meet Microfluidics: From Stable Emulsions to Photoinduced Synthesis of Hollow Polymer Spheres. *Small* **2020**, *16*, 2001180.

(17) Cao, Q.; Barrio, J.; Antonietti, M.; Kumru, B.; Shalom, M.; Schmidt, B. V. K. J. Photoactive Graphitic Carbon Nitride-Based Gel Beads As Recyclable Photocatalysts. *ACS Appl. Polym. Mater.* **2020**, *2*, 3346−3354.

(18) Cao, Q.; Kumru, B. Polymeric Carbon Nitride Armored Centimeter-Wide Organic Droplets in Water for All-Liquid Heterophase Emission Technology. *Polymers* **2020**, *12*, 1626.

(19) Cao, Q.; Kumru, B.; Antonietti, M.; Schmidt, B. V. K. J. Grafting Polymers onto Carbon Nitride via Visible-Light-Induced Photofunctionalization. *Macromolecules* **2019**, *52*, 4989−4996.

(20) Barrio, J.; Shalom, M. Rational Design of Carbon Nitride Materials by Supramolecular Preorganization of Monomers. *ChemCatChem* **2018**, *10*, 5573−5586.
(21) Li, B.; Si, Y.; Fang, Q.; Shi, Y.; Huang, W. Q.; Hu, W.; Pan, A.; Fan, X.; Huang, G. F. Hierarchical Self-assembly of Well-Defined Louver-Like P-Doped Carbon Nitride Nanowire Arrays with Highly Efficient Hydrogen Evolution. *Nano-Micro Lett.* **2020**, *12*, 52.
(22) Chen, Y.; He, X.; Guo, D.; Cai, Y.; Chen, J.; Zheng, Y.; Gao, B.; Lin, B. Supramolecular electrostatic self-assembly of mesoporous thin-walled graphitic carbon nitride microtubes for highly efficient visible-light photocatalytic activities. *J. Energy Chem.* **2020**, *49*, 214−223.
(23) Fettkenhauer, C.; Weber, J.; Antonietti, M.; Dontsova, D. Novel carbon nitride composites with improved visible light absorption synthesized in ZnCl2-based salt melts. *RSC Adv.* **2014**, *4*, 40803−40811.
(24) Miller, T. S.; Suter, T. M.; Telford, A. M.; Picco, L.; Payton, O. D.; Russell-Pavier, F.; Cullen, P. L.; Sella, A.; Shaffer, M. S. P.; Nelson, J.; Tileli, V.; McMillan, P. F.; Howard, C. A. Single Crystal, Luminescent Carbon Nitride Nanosheets Formed by Spontaneous Dissolution. *Nano Lett.* **2017**, *17*, 5891−5896.
(25) Guo, S.; Deng, Z.; Li, M.; Jiang, B.; Tian, C.; Pan, Q.; Fu, H. Phosphorus-Doped Carbon Nitride Tubes with a Layered Micronanostructure for Enhanced Visible-Light Photocatalytic Hydrogen Evolution. *Angew. Chem., Int. Ed.* **2016**, *55*, 1830−1834.
(26) Villa, K.; Manzanares Palenzuela, C. L.; Sofer, Z.; Matějková, S.; Pumera, M. Metal-Free Visible-Light Photoactivated C_3N_4 Bubble-Propelled Tubular Micromotors with Inherent Fluorescence and On/Off Capabilities. *ACS Nano* **2018**, *12*, 12482−12491.
(27) Kumru, B.; Antonietti, M. Colloidal properties of the metal-free semiconductor graphitic carbon nitride. *Adv. Colloid Interface Sci.* **2020**, *283*, 102229.
(28) Hasija, V.; Raizada, P.; Sudhaik, A.; Sharma, K.; Kumar, A.; Singh, P.; Jonnalagadda, S. B.; Thakur, V. K. Recent advances in noble metal free doped graphitic carbon nitride based nanohybrids for photocatalysis of organic contaminants in water: A review. *Appl. Mater. Today* **2019**, *15*, 494−524.
(29) Shiraishi, Y.; Kofuji, Y.; Kanazawa, S.; Sakamoto, H.; Ichikawa, S.; Tanaka, S.; Hirai, T. Platinum nanoparticles strongly associated with graphitic carbon nitride as efficient co-catalysts for photocatalytic hydrogen evolution under visible light. *Chem. Commun.* **2014**, *50*, 15255−15258.
(30) Ghosh, K.; Kumar, M.; Wang, H.; Maruyama, T.; Ando, Y. Facile Decoration of Platinum Nanoparticles on Carbon-Nitride Nanotubes via Microwave-Assisted Chemical Reduction and Their Optimization for Field-Emission Application. *J. Phys. Chem. C* **2010**, *114*, 5107−5112.
(31) Singh, J. A.; Overbury, S. H.; Dudney, N. J.; Li, M.; Veith, G. M. Gold Nanoparticles Supported on Carbon Nitride: Influence of Surface Hydroxyls on Low Temperature Carbon Monoxide Oxidation. *ACS Catal.* **2012**, *2*, 1138−1146.
(32) Chen, L.; Zeng, X.; Si, P.; Chen, Y.; Chi, Y.; Kim, D.-H.; Chen, G. Gold Nanoparticle-Graphite-Like C_3N_4 Nanosheet Nanohybrids Used for Electrochemiluminescent Immunosensor. *Anal. Chem.* **2014**, *86*, 4188−4195.
(33) Zhao, G.; Huang, X.; Wang, X.; Wang, X. Progress in catalyst exploration for heterogeneous CO_2 reduction and utilization: a critical review. *J. Mater. Chem. A* **2017**, *5*, 21625−21649.
(34) Yang, Y.; Zeng, G.; Huang, D.; Zhang, C.; He, D.; Zhou, C.; Wang, W.; Xiong, W.; Song, B.; Yi, H.; Ye, S.; Ren, X. In Situ Grown Single-Atom Cobalt on Polymeric Carbon Nitride with Bidentate Ligand for Efficient Photocatalytic Degradation of Refractory Antibiotics. *Small* **2020**, *16*, 2001634.
(35) Zhang, W.; Peng, Q.; Shi, L.; Yao, Q.; Wang, X.; Yu, A.; Chen, Z.; Fu, Y. Merging Single-Atom-Dispersed Iron and Graphitic Carbon Nitride to a Joint Electronic System for High-Efficiency Photocatalytic Hydrogen Evolution. *Small* **2019**, *15*, 1905166.
(36) Chen, Z.; Pronkin, S.; Fellinger, T.-P.; Kailasam, K.; Vilé, G.; Albani, D.; Krumeich, F.; Leary, R.; Barnard, J.; Thomas, J. M.; Pérez-Ramírez, J.; Antonietti, M.; Dontsova, D. Merging Single-Atom-Dispersed Silver and Carbon Nitride to a Joint Electronic System via Copolymerization with Silver Tricyanomethanide. *ACS Nano* **2016**, *10*, 3166−3175.
(37) Brandi, F.; Bäumel, M.; Molinari, V.; Shekova, I.; Lauermann, I.; Heil, T.; Antonietti, M.; Al-Naji, M. Nickel on nitrogen-doped carbon pellets for continuous-flow hydrogenation of biomass-derived compounds in water. *Green Chem.* **2020**, *22*, 2755−2766.
(38) Zhang, G.; Lan, Z.-A.; Wang, X. Surface engineering of graphitic carbon nitride polymers with cocatalysts for photocatalytic overall water splitting. *Chem. Sci.* **2017**, *8*, 5261−5274.
(39) Jin, Z.; Murakami, N.; Tsubota, T.; Ohno, T. Complete oxidation of acetaldehyde over a composite photocatalyst of graphitic carbon nitride and tungsten(VI) oxide under visible-light irradiation. *Appl. Catal., B* **2014**, *150−151*, 479−485.
(40) Ohno, T.; Murakami, N.; Koyanagi, T.; Yang, Y. Photocatalytic reduction of CO_2 over a hybrid photocatalyst composed of WO_3 and graphitic carbon nitride ($g\text{-}C_3N_4$) under visible light. *J. CO2 Util.* **2014**, *6*, 17−25.
(41) Kailasam, K.; Fischer, A.; Zhang, G.; Zhang, J.; Schwarze, M.; Schröder, M.; Wang, X.; Schomäcker, R.; Thomas, A. Mesoporous Carbon Nitride-Tungsten Oxide Composites for Enhanced Photocatalytic Hydrogen Evolution. *ChemSusChem* **2015**, *8*, 1404−1410.
(42) Li, K.; Yan, L.; Zeng, Z.; Luo, S.; Luo, X.; Liu, X.; Guo, H.; Guo, Y. Fabrication of $H_3PW_{12}O_{40}$-doped carbon nitride nanotubes by one-step hydrothermal treatment strategy and their efficient visible-light photocatalytic activity toward representative aqueous persistent organic pollutants degradation. *Appl. Catal., B* **2014**, *156−157*, 141−152.
(43) Ding, J.; Wang, L.; Liu, Q.; Chai, Y.; Liu, X.; Dai, W.-L. Remarkable enhancement in visible-light absorption and electron transfer of carbon nitride nanosheets with 1% tungstate dopant. *Appl. Catal., B* **2015**, *176−177*, 91−98.
(44) Thaweesak, S.; Wang, S.; Lyu, M.; Xiao, M.; Peerakiatkhajohn, P.; Wang, L. Boron-doped graphitic carbon nitride nanosheets for enhanced visible light photocatalytic water splitting. *Dalton Trans.* **2017**, *46*, 10714−10720.
(45) Zhang, Y.; Mori, T.; Ye, J.; Antonietti, M. Phosphorus-Doped Carbon Nitride Solid: Enhanced Electrical Conductivity and Photocurrent Generation. *J. Am. Chem. Soc.* **2010**, *132*, 6294−6295.
(46) Rajkumar, C.; Veerakumar, P.; Chen, S.-M.; Thirumalraj, B.; Lin, K.-C. Ultrathin Sulfur-Doped Graphitic Carbon Nitride Nanosheets As Metal-Free Catalyst for Electrochemical Sensing and Catalytic Removal of 4-Nitrophenol. *ACS Sustainable Chem. Eng.* **2018**, *6*, 16021−16031.
(47) Rao, K. T. V.; Prasad, P. S. S.; Lingaiah, N. Solvent-free hydration of alkynes over a heterogeneous silver exchanged silicotungstic acid catalyst. *Green Chem.* **2012**, *14*, 1507−1514.
(48) Varisli, D.; Dogu, T.; Dogu, G. Silicotungstic Acid Impregnated MCM-41-like Mesoporous Solid Acid Catalysts for Dehydration of Ethanol. *Ind. Eng. Chem. Res.* **2008**, *47*, 4071−4076.
(49) Simsek, V.; Degirmenci, L.; Murtezaoglu, K. Synthesis of a silicotungstic acid SBA-15 catalyst for selective monoglyceride production. *React. Kinet., Mech. Catal.* **2016**, *117*, 773−788.
(50) Ramalingam, M.; Manickam, S.; Srinivasalu, K. R.; Ismail, M. B.; Deivanayagam, E. Ionic Immobilization of Silicotungstic Acid on Amine-Functionalized Zirconia: A Mesoporous Catalyst for Esterification of Maleic Acid. *Eur. J. Inorg. Chem.* **2016**, *2016*, 1697−1705.
(51) Srivani, A.; Venkateswar Rao, K. T.; Sai Prasad, P. S.; Lingaiah, N. An efficient synthesis of benzoxazoles using silica-supported tin exchanged silicotungstic acid catalyst. *J. Mol. Catal. A: Chem.* **2010**, *328*, 119−123.
(52) Liang, Y.-C.; Chang, C.-W. Preparation of Orthorhombic WO_3 Thin Films and Their Crystal Quality-Dependent Dye Photodegradation Ability. *Coatings* **2019**, *9*, 90.
(53) Sun, Z.; Wang, W.; Chen, Q.; Pu, Y.; He, H.; Zhuang, W.; He, J.; Huang, L. A hierarchical carbon nitride tube with oxygen doping and carbon defects promotes solar-to hydrogen conversion. *J. Mater. Chem. A* **2020**, *8*, 3160−3167.

(54) Fan, M.; Cui, J.; Wu, J.; Vajtai, R.; Sun, D.; Ajayan, P. M. Improving the Catalytic Activity of Carbon-Supported Single Atom Catalysts by Polynary Metal or Heteroatom Doping. *Small* **2020**, *16*, 1906782.
(55) Zhu, B.; Xia, P.; Li, Y.; Ho, W.; Yu, J. Fabrication and photocatalytic activity enhanced mechanism of direct Z-scheme g-C_3N_4/Ag_2WO_4 photocatalyst. *Appl. Surf. Sci.* **2017**, *391*, 175−183.
(56) Cruz, D.; Garcia Cerrillo, J.; Kumru, B.; Li, N.; Dario Perea, J.; Schmidt, B. V. K. J.; Lauermann, I.; Brabec, C. J.; Antonietti, M. Influence of Thiazole-modified Carbon Nitride Nanosheets with Feasible Electronic Properties on Inverted Perovskite Solar Cells. *J. Am. Chem. Soc.* **2019**, *141*, 12322−12328.
(57) Kumru, B.; Cruz, D.; Heil, T.; Schmidt, B. V. K. J.; Antonietti, M. Electrostatic Stabilization of Carbon Nitride Colloids in Organic Solvents Enables Stable Dispersions and Transparent Homogeneous CN-Films for Optoelectronics. *J. Am. Chem. Soc.* **2018**, *140*, 17532−17537.
(58) Li, X.-H.; Antonietti, M. Metal nanoparticles at mesoporous N-doped carbons and carbon nitrides: functional Mott−Schottky heterojunctions for catalysis. *Chem. Soc. Rev.* **2013**, *42*, 6593−6604.
(59) Zhan, F.; Xie, R.; Li, W.; Li, J.; Yang, Y.; Li, Y.; Chen, Q. In situ synthesis of g-C_3N_4/WO_3 heterojunction plates array films with enhanced photoelectrochemical performance. *RSC Adv.* **2015**, *5*, 69753−69760.
(60) Abbas, S. C.; Wu, J.; Huang, Y.; Babu, D. D.; Anandhababu, G.; Ghausi, M. A.; Wu, M.; Wang, Y. Novel strongly coupled tungsten-carbon-nitrogen complex for efficient hydrogen evolution reaction. *Int. J. Hydrogen Energy* **2018**, *43*, 16−23.
(61) McCleverty, J. A. Tungsten: Inorganic&Coordination Chemistry. In *Encyclopedia of Inorganic Chemistry*, 2 ed.; King, R. B., Ed. John Wiley & Sons, Ltd., 2006.
(62) Zhou, N.; Wang, N.; Wu, Z.; Li, L. Probing Active Sites on Metal-Free, Nitrogen-Doped Carbons for Oxygen Electroreduction: A Review. *Catalysts* **2018**, *8*, 509.
(63) Wang, Y. L.; Nie, T.; Li, Y. H.; Wang, X. L.; Zheng, L. R.; Chen, A. P.; Gong, X. Q.; Yang, H. G. Black Tungsten Nitride as a Metallic Photocatalyst for Overall Water Splitting Operable at up to 765 nm. *Angew. Chem., Int. Ed.* **2017**, *56*, 7430−7434.
(64) Tobimatsu, Y.; Schuetz, M. Lignin polymerization: how do plants manage the chemistry so well? *Curr. Opin. Biotechnol.* **2019**, *56*, 75−81.
(65) Simmons, K. E.; Minard, R. D.; Bollag, J.-M. Oxidative Coupling and Polymerization of Guaiacol, a Lignin Derivative. *Soil Sci. Soc. Am. J.* **1988**, *52*, 1356−1360.
(66) Wilkesman, J.; Castro, D.; Contreras, L. M.; Kurz, L. Guaiacol peroxidase zymography for the undergraduate laboratory. *Biochem. Mol. Biol. Educ.* **2014**, *42*, 420−426.
(67) Lazaridis, P. A.; Fotopoulos, A. P.; Karakoulia, S. A.; Triantafyllidis, K. S. Catalytic Fast Pyrolysis of Kraft Lignin With Conventional, Mesoporous and Nanosized ZSM-5 Zeolite for the Production of Alkyl-Phenols and Aromatics. *Front. Chem.* **2018**, *6*, 295.